

Terrestrial Water storage

Manuela Girotto^{1,2} and Matt Rodell³

¹ Global Modeling and Assimilation Office, NASA Goddard Space Flight Center, Greenbelt, MD, USA

² GESTAR, Universities Space Research Association, Columbia, MD 21044, USA

³ Hydrological Science Lab, NASA Goddard Space Flight Center, Greenbelt, MD, USA

Abstract

Terrestrial water storage can be defined as the summation of all water on the land surface and in the subsurface. It includes surface soil moisture, root zone soil moisture, groundwater, snow, ice, water stored in the vegetation, river and lake water. Terrestrial water storage (TWS) changes have been observed by the Gravity Recovery and Climate Experiment (GRACE) mission since 2002. GRACE has provided an unprecedented view of the terrestrial water storage variations at large scales. Extremes in water storage often are associated with droughts and flooding events because they are driven by the surplus or deficit of water. Few hydrologic observing networks yield sufficient data for comprehensive monitoring of changes in the total amount of water stored in a region. GRACE observations have helped to fill this gap. This book chapter is divided into 4 sections. Section 1 provides an overview of the GRACE mission. Section 2 reviews the terrestrial water storage solutions that are available. Section 3 describes regional to global applications of GRACE for monitoring extremes in the terrestrial water storage, including droughts and flooding events. Conclusions and future directions are reported in Section 4.

Key words:

1. GRACE

- 25 2. water storage
- 26 3. droughts
- 27 4. floods
- 28 5. terrestrial water storage
- 29 6. groundwater
- 30

31 **0. Terrestrial Water Storage**

32 Terrestrial water storage (TWS) is a dynamic component of the hydrological cycle that
33 exerts important controls over the water, energy and biogeochemical fluxes, thereby playing a
34 major role in Earth's climate system (Syed et al., 2008; Famiglietti, 2004). TWS is defined as the
35 summation of all water stored above and below the land surface. This includes surface waters, soil
36 moisture, groundwater, snow and ice and water stored in vegetation. The variability of TWS tends
37 to be dominated by surface waters in wet, tropical regions such as the Amazon, by soil moisture and
38 groundwater in mid-latitudes, and by snow and ice in polar and alpine regions (Rodell and
39 Famiglietti, 2001). The variations in water stored in vegetation are small compared to those of the
40 other TWS components, therefore they are typically assumed to be negligible in TWS budget
41 analyses (Rodell et al., 2005).

42 Surface waters include rivers, inland water bodies, wetlands and inundated floodplains.
43 Surface waters supply agricultural and energy production for most regions in the tropics, and
44 because they exist at the land-atmosphere interface they affect hydrometeorological and
45 biogeochemical processes. Getirana et al. (2017) found that changes in surface water storage are a
46 substantial component of TWS variability in the wet tropics (e.g., the Amazon), where major rivers
47 flow over arid regions (e.g., the Nile River in Egypt) and in sub-polar regions. Conversely, changes in
48 surface water storage are negligible in the Western U.S., Northern Africa, Middle East, and central
49 Asia.

50 Soil moisture is defined as the water stored in the unsaturated zone of the soil. It controls
51 the partitioning of rainfall into runoff and infiltration, constrains evapotranspiration, and influences
52 the occurrence of flood water extremes, because when the soil is saturated it cannot infiltrate
53 anymore water (Milly and Dunne, 1994; Crow et al., 2005; Zehe et al., 2005). Soil moisture governs
54 the partitioning of the turbulent fluxes (latent and sensible heat) hence it affects global and regional
55 hydrometeorological processes (Entekhabi et al., 1996; Seneviratne et al., 2010). In parts of the

56 tropics and in the midlatitudes, soil moisture variations are generally the largest component of
57 seasonal terrestrial water storage changes.

58 Groundwater is the other major component of TWS in the midlatitudes, where provides
59 domestic water to a billion people and plays a central role in agriculture and energy production
60 (Gleeson et al., 2012; Famiglietti, 2014). This resource has received increased attention in recent
61 years because of the accelerated rate of depletion of major global aquifers (E.g., Rodell et al., 2009;
62 Wada et al., 2010; Famiglietti et al., 2011; Richey et al., 2015; Giroto et al., 2017). Groundwater
63 storage changes are rarely the dominant component of TWS variations on a seasonal basis, but they
64 are often the dominant component on interannual to decadal timescales (Rodell and Famiglietti,
65 2001; Li et al., 2015).

66 Finally, the water stored in form of snow or ice is the primary component of TWS in high
67 latitude regions and mountainous regions of the mid-latitudes (Rodell and Famiglietti, 2001;
68 Seneviratne et al., 2003; Getirana et al., 2017). This is because snow water storage induces
69 significant variations in TWS due to the mass that accumulates during winter and the mass that
70 melts during springtime. These fluctuations also affect the surface energy balance because of the
71 changes in surface albedo (Hall 1988). Accurate global estimates of snow across space and time are
72 currently lacking due to complexity of the terrain or inaccessibility of the regions where snow/ice is
73 stored. For this reason, large-scale efforts for estimating snow properties must heavily rely on
74 remote sensing (Schmugge et al., 2002; Giroto et al., 2014). Existing efforts to estimate snow water
75 equivalent (SWE) from remote sensing include using microwave, visible and near infrared, radar
76 and gravimetric measurements. A dedicated snow-measuring satellite mission has not yet been
77 launched, but efforts have begun (e.g., NASA SnowEx, <https://snow.nasa.gov/campaigns/snowex>)
78 in which international teams of experts are working to devise satellite instruments capable of
79 measuring SWE and/or snow depth from space.

80

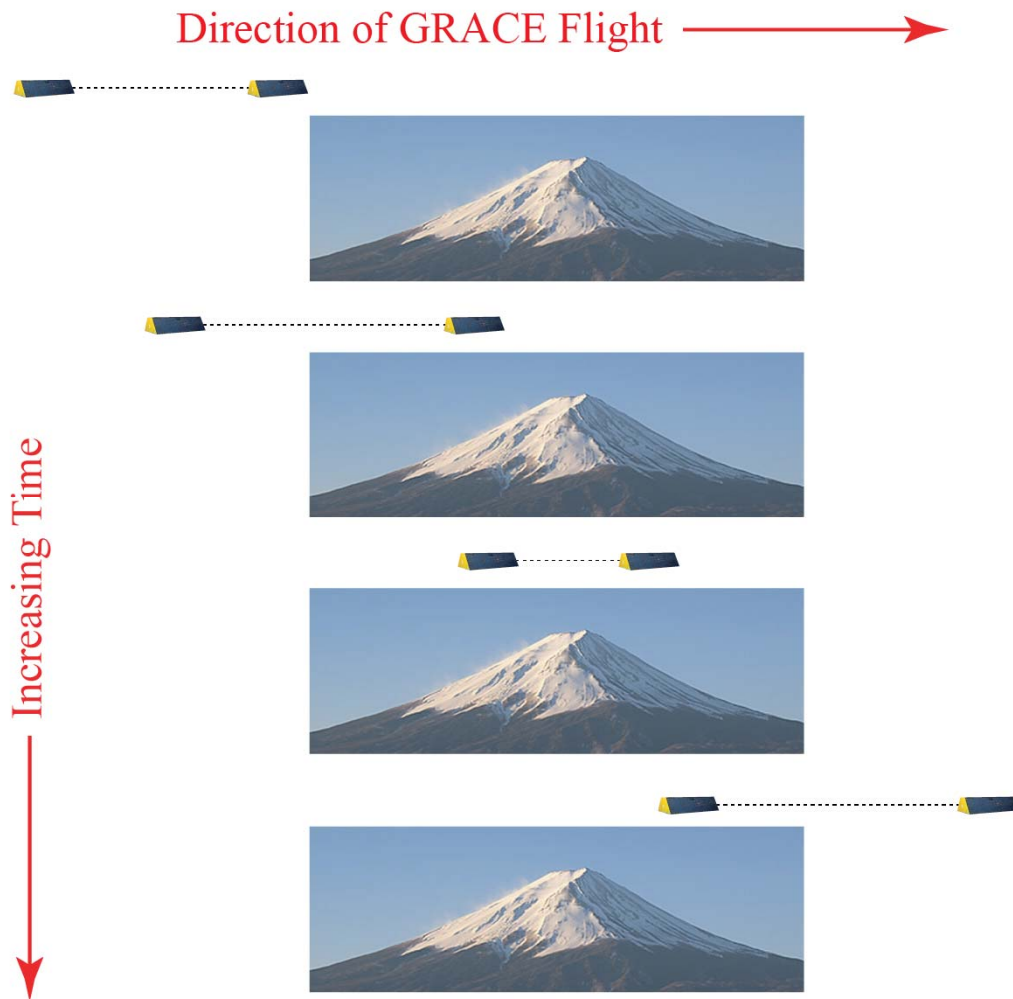
81

82 **1. Overview of the GRACE mission**

83 The Gravity Recovery and Climate Experiment (GRACE) maps the gravity potential of the
84 Earth. From these gravity maps scientists can infer global and regional changes of the terrestrial
85 water storage, ice loss, and sea level change caused by the addition of water to the ocean providing
86 a unique view of Earth's climate and have far-reaching benefits to society and the world's
87 population. GRACE is jointly operated by NASA and the German Aerospace Center. It was launched
88 on March 17 2002, and it continued to perform past its nominal mission lifetime of 5 years until
89 battery failure caused the end of the science mission in 2017. It consisted of two satellites in a
90 tandem orbit about 200 km apart at 450–500 km altitude. **Figure 1** shows in a simplistic way the
91 principle behind the gravity measurements. The two GRACE satellites flew in a tandem orbit over
92 the Earth. In the case shown in **Figure 1**, a mountain represents a positive mass anomaly. As the
93 lead satellite approached the mountain it was pulled toward it because of the gravitational force
94 exerted by the mass anomaly. Thus, the distance between the two satellites increased. As the
95 trailing satellite approached the mountain, it was pulled toward the anomalous mass while the lead
96 satellite was held back by the same mass anomaly, and the distance between the satellites
97 decreased. Finally, as the trailing satellite moved away from the mountain, it was held back, and
98 their distance increased again. In a nutshell, measurement of the distance (range) and changes in
99 distance (range-rate) between the two satellites are related to the gravitational potential of earth
100 masses. A K-band microwave tracking system continuously measures changes in the distance
101 between the satellites with a precision better than 1 μm (Tapley et al., 2004). The measurements
102 are so precise that mass changes associated with ocean circulation, atmospheric circulation, and
103 terrestrial water storage redistribution can be detected by GRACE. Nongravitational accelerations
104 are monitored by onboard accelerometers, and the precise positions of the satellites are measured
105 via global positioning system (GPS). The monthly analysis of the range and range-rate

106 measurements between the two satellites provides the temporal variations (i.e., anomalies) of the
107 gravity field.

108 The successor of GRACE is the GRACE follow-on (GRACE-FO) mission. GRACE-FO, launched
109 on May 22 2018, carries on the work of its predecessor while testing a new laser ranging system
110 designed to improve the precision of the intersatellite distance measurement.



111

112 **Figure 1. Simplified example of how the GRACE mission observed the time variable gravity field. The**
113 **two GRACE satellites flew in tandem over the Earth (first panel). In this graphic the mountain**
114 **represents a positive mass anomaly. As the lead satellite approached the mountain it was pulled**
115 **toward it because of the gravitational force exerted by the mass anomaly. Thus, the distance between**
116 **the two satellites increased (second panel). As the trailing satellite approached the mountain, it was**
117 **pulled toward the anomalous mass while the lead satellite was held back by the same mass anomaly,**
118 **and the distance between the satellites decreased (third panel). Finally, as the trailing satellite moved**
119 **away from the mountain, it was held back, and their distance increased again (fourth panel).**

120 **2. Terrestrial Water Storage Solutions**

121 A monthly analysis of the range and range-rate measurements results in a map of temporal
122 variations (i.e., anomalies) of the gravity fields caused by redistribution of earth masses. Masses can
123 be static or time variable. Static masses include the total mass of the earth and mass heterogeneities
124 that only vary on geologic time scales. This includes location of the continents, mountains, and
125 depression in the crust. The static masses are “removed” when the long term mean gravity field is
126 saturated from a month solution to produce an anomaly map. The main drivers of temporal
127 variations in the gravity field are oceanic and atmospheric circulations and redistribution of
128 terrestrial water via the hydrological cycle. Atmosphere mass changes are removed during pre-
129 processing using model based atmospheric pressure fields. An ocean model is used to remove high
130 frequency (6-hourly to sub-monthly) wind and pressure-driven ocean motions that might
131 otherwise alias into the monthly gravity solutions. What remains are anomalies in terrestrial water
132 storage (TWS). Glacial isostatic adjustment must also be considered in certain regions such as
133 Hudson’s Bay in Canada, and a major earthquake can produce a significant gravitational anomaly,
134 but the timescales of most solid earth processes are too long to be an issue.

135 Currently, the range-rate observations are processed using either spherical harmonics
136 (Wahr et al., 1998) or the mass concentration (mascon, Rowlands et al., 2005) approach to produce
137 the monthly gravity solutions.

138 The spherical harmonics solutions represent the gravity field via a set of coefficients
139 (degree and order ≤ 120) of a given spherical harmonic expansion that describes the shape of the
140 geoid (the surface of constant gravitational potential best matching the mean sea surface). The
141 expansion coefficients can be manipulated using numerical devices such as Gaussian averaging
142 functions in order to isolate mass anomalies (deviations from the baseline temporal mean) over
143 regions of interest (e.g., Wahr et al., 1998). The spherical harmonic solutions have typically suffered
144 from poor observability of east-west gradients, resulting in the so-called “stripes” that are

145 conventionally removed via empirical smoothing and/or “destriping” algorithms (Swensen and
146 Wahr 2006). Although quite effective, especially for larger spatial scales, the destriping also
147 removes some real geophysical signal along with the stripes, and the size, shape, and orientation of
148 the signals strongly affects the effectiveness of destriping (Watkins et al., 2015). For this reason,
149 errors in such estimates are inversely related to the size of the region, being as small as 1–2 cm
150 equivalent height of water over continental-scale river basins, and being large enough to
151 overwhelm the hydrology signal as the area drops below $\sim 150,000 \text{ km}^2$ (Rodell and Famiglietti,
152 1999, Wahr et al., 2006). Three centers are currently generating spherical harmonic fields: the
153 Center for Space Research at the University of Texas; the GeoForschungsZentrum. Potsdam,
154 Germany; and the Jet Propulsion Laboratory, California.

155 As an alternative to the spherical harmonic technique, the inter-satellite ranging data can
156 also be used directly to estimate regional “mass concentrations” (mascons) without the need to first
157 derive a global gravity field (Rowlands et al., 2005). The primary advantage of using mascons as a
158 basis function is that each mascon has a specific known geophysical location (unlike spherical
159 harmonic coefficients which individually have no particular localization information). Mascons take
160 advantage of this convenient property to specify a-priori information (constraints) during the data
161 inversion to internally remove the correlated error in the gravity solution. So, unlike the spherical
162 harmonic solutions, the constrained mascon solutions typically do not need to be destriped or
163 smoothed. The mascon approach also allows a better separation of land and ocean signals. Mascons
164 solutions are currently freely available from different centers such as the Jet Propulsion Laboratory,
165 California (Watkins et al., 2015); the Goddard Space and Flight Center, Maryland (Luthcke et al.,
166 2013); and the Center for Space Research, Texas (Save et al., 2012).

167

168 **3. Extremes in Water Storage**

169 Extremes in water storage often are manifested as droughts and flooding events, driven by
170 the surplus or deficit of water stored in a river basin or an aquifer. Understanding the spatial and
171 temporal extend of these hydrologic extremes is critical for water resources management, hazard
172 preparedness, and food security (Differbaugh and Scheree 2011; D’Odorico et al., 2010). Few
173 hydrologic observing networks yield sufficient data for comprehensive monitoring of changes in
174 the total amount of water stored in a region (Rodell and Famiglietti, 2001). GRACE observations
175 have helped to fill this gap. They have been used to characterize regional flood potential (e.g.,
176 Reager and Famiglietti 2009) and to assess wetness and drought for the U.S. Drought Monitor (e.g.,
177 Houburg et al., 2012). Further, as an integrated measure of all surface and groundwater storage
178 changes, GRACE data implicitly contains a record of seasonal to interannual water storage
179 variations that can likely be exploited to lengthen early warning periods for regional flood and
180 drought prediction (Thomas et al., 2014, Sun et al., 2017). The next two subsections will provide a
181 review of the extreme water storage events identified by the GRACE mission along with the
182 potential for predictability.

183

184 **3.1 Droughts**

185 Meteorological drought is defined as an extended period of low precipitation, whereas
186 hydrological droughts are generally defined as extended periods of water storage deficits leading to
187 low streamflow. Satellite gravimetry is the only remote sensing technique able to monitor the water
188 storage in a holistic manner. For this reason, GRACE data have been investigated alone, or in
189 combination with land surface models, to analyze worldwide hydrological drought conditions and
190 provide new methods to monitor droughts (Li et al., submitted, Zhao et al., 2017). Further, GRACE
191 can contribute to regional drought characterization by measuring water storage deficits in
192 previously identified, drought-stricken areas. The duration and magnitude of the deficits can serve

193 as metrics to help quantify hydrological drought severity (Thomas et al., 2014). This subsection
194 provides a review of previous studies that used GRACE to quantify, analyze, and monitor droughts.

195 Recent studies have investigated the potential for using GRACE information to monitor
196 droughts. In addition to Thomas et al. (2014) and Houburg et al. (2012), Cao et al. (2015)
197 introduced the total storage deficit index, derived from the GRACE-recovered terrestrial water
198 storage changes, to analyze drought characteristics in arid Northwestern China. Yirdaw et al.
199 (2008) employed the total storage deficit index, to characterize the 2002/2003 drought episode
200 and generate a pictorial representation of the long-term dryness and wetness within the
201 Saskatchewan River Basin in Canada. Yi and Wen (2016) established a GRACE-based hydrological
202 drought index for drought monitoring in the continental United States from 2003 to 2012. Kusche
203 et al. (2016) mapped the probabilities of extreme continental water storage changes from space
204 gravimetry. They derived hot spot regions of high probability of peak anomalous water storage.
205 Using the GRACE-derived TWS anomaly index, Wang et al. (2014) compared the precipitation
206 anomaly index and the vegetation anomaly index to analyze the drought events in the Haihe River
207 Basin, China, from January 2003 to January 2013. Thomas et al. (2014) described a quantitative
208 approach (based on water storage deficits) to measure the occurrence, severity, frequency,
209 magnitude, and duration of hydrological droughts based on the GRACE-derived TWS (Sun et al.,
210 2018).

211 Combined satellite/model drought monitoring tools are also becoming more common. Data
212 assimilation systems merge observations with physically based models, using the model to provide
213 spatially and temporally complete estimates of all drought-relevant hydrologic variables and the
214 observation record to correct for model errors (Anderson et al., 2012). In particular, the application
215 of the GRACE data assimilation approach for drought monitoring has recently been explored by
216 NASA-funded investigations (Houburg et al., 2012, Rodell 2012). These result in surface and root-
217 zone soil moisture and groundwater drought indicators based on GRACE data assimilation results,

218 and to evaluation of those indicators as inputs to the USDM products. Houborg et al. (2012) and Li
219 et al. (2012) use GRACE data assimilation to evaluate its potential for developing new drought
220 indicator products to serve as baselines for the Drought Monitor maps. The assimilation
221 downscaled (in space and time) and disaggregated GRACE data into finer scale components of TWS,
222 which exhibited significant changes in their dryness rankings relative to those without data
223 assimilation, suggesting that GRACE data assimilation could have a substantial impact on drought
224 monitoring (Li et al., 2012, Houborg et al., 2012). The weekly indicators are available on the National
225 Drought Mitigation Center's website (<http://drought.unl.edu>).

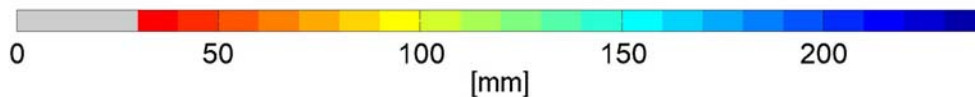
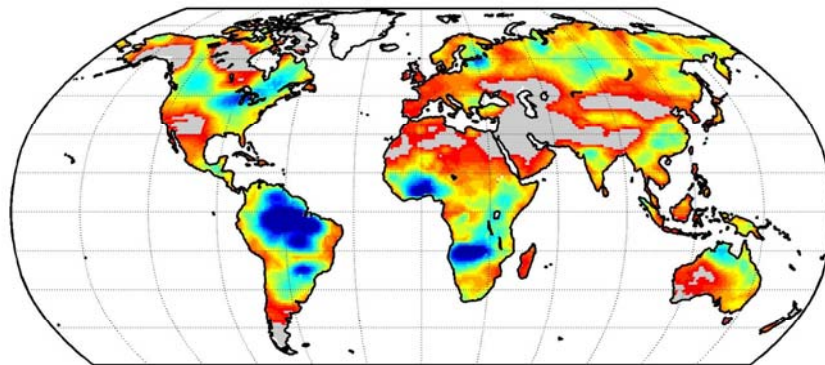
226

227 *3.1.1 Major World Droughts*

228 Thomas et al. (2014) present gravity-based measurements of water storage anomalies
229 during recent droughts. They use GRACE to explore how hydrological droughts may be better
230 characterized while estimating the associated regional water storage deficit. The average storage
231 deficit during drought events can be identified using the 1) storage deficit as a negative departure
232 from the seasonal cycle and 2) the drought duration as the number of months with continuous
233 deficits (Thomas et al., 2014). In essence, the average storage deficit is an arithmetic mean of the
234 storage deficit observed during a given drought event and it is used as a measure of drought
235 intensity. Based on these definitions of storage deficit and drought duration, Humphrey et al.
236 (2016) provide a review of all drought events identified in the GRACE period from 2002-2015.
237 **Figure 2** shows the maximum average storage deficit ever observed for all drought events
238 identified in the April 2002-January 2017 by the GRACE record as derived by Humphrey et al.
239 (2016). The year corresponding to this maximum is depicted in **Figure 2b**. Here, we group these
240 major drought events by continents. Further, we discuss on potential for using GRACE data and
241 models (via data assimilation) to improve predictability of these droughts events (Section 3.1.2).

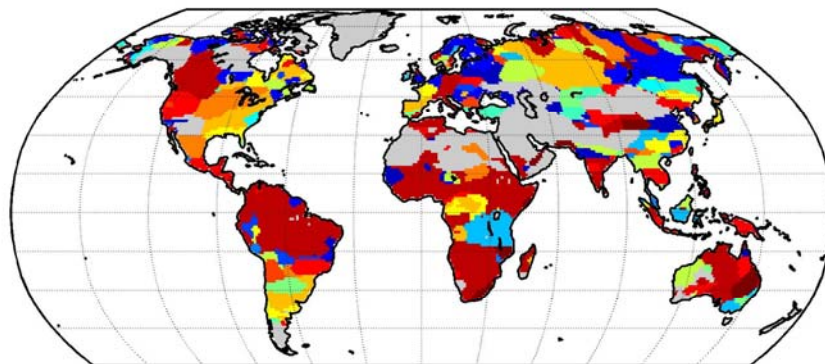
242

Maximum average storage deficits



244

Year of the maximum



245

246 **Figure 2. a) Maximum value of the average storage deficit observed in the period April 2002–August**
 247 **2015, expressed in mm of equivalent water height. b) Year corresponding to the maximum value of**
 248 **the average storage deficit, showing only regions with a deficit larger than 30 mm (adapted from**
 249 **Humphrey et al., 2016).**

250

251 *South America*

252 The Amazon River water storage during year 2016 was one of the lowest during the GRACE
 253 record (**Figure 2**). Other droughts, not shown, are identified for this region, such as the 2004-2008,
 254 and 2010 dry-period reported in the work by Humphrey et al., (2016), Frappart et al. (2012) and

255 Thomas et al. (2014). Getirana (2016) uses GRACE to identify a water loss rate of 26.1 cm/year for
256 southeastern Brazil over the period from 2012 to 2015. Drought events in the Amazon River basin
257 were shown to be related to precipitation deficits and to the El Niño Southern Oscillation (ENSO,
258 Davidson et al. 2012; Frappart et al. 2012). The Amazon basin extreme droughts cause ineffective
259 hydropower production. In fact, water storage droughts in this region cause massive agricultural
260 losses, water supply restrictions, and energy rationing.

261 The 2008-2012 La Plata basin (Argentina) drought is also seen in **Figure 2**. Chen et al.,
262 (2010) identify the onset of this drought using GRACE. In their work, GRACE revealed details of the
263 temporal and spatial evolution of this drought, with onset around austral spring 2008 in the lower
264 La Plata basin, which spread to the entire La Plata basin. Wetness and drought in this region is
265 correlated with ENSO, with dry and wet seasons corresponding to ENSO events, respectively (Chen
266 et al., 2010, Abelen et al. 2015; Sordo-Ward et al., 2017).

267

268 North America

269 The 2012-2015 drought in the Central Valley of California is also seen in **Figure 2**. This
270 drought reduced natural recharge to the aquifers and caused low annual snow accumulations in the
271 Sierra Nevada Mountains (Margulis et al., 2016). Further, groundwater acts as the key strategic
272 reserve in times of drought and the Central Valley is the most productive agricultural region for
273 fresh produce in the USA (Faunt 2009). Excessive groundwater pumping during a period of
274 meteorological drought can cause unrecoverable losses at aquifer storage capacity (Faunt 2009;
275 Famiglietti et al., 2011; Famiglietti 2014; Scanlon et al. 2012a,b). For example, Famiglietti et al.
276 (2011) estimate a depletion in groundwater that totaled of 20 km³ of water during 2012-2015.
277 Continued groundwater depletion at this rate may well be unsustainable, with potentially dire
278 consequences for the economic and food security of the United States (Famiglietti et al., 2011).
279 Groundwater depletion can cause significant land subsidence (Galloway et al. 1999). The analysis of

280 TWS for the entire GRACE record also indicates dry episodes for previous years over the
281 southwestern United States. For example, Scanlon et al (2012a) and Famiglietti et al., (2011) report
282 that groundwater depletion was observed in the Central Valley during the drought period from
283 April 2006 through September 2009.

284 Notably, most of the United States, experienced droughts in 2012 (**Figure 2**). The U.S.
285 Drought Monitor (Svuboda et al., 2002) estimated that over three-quarters of the contiguous United
286 States experienced at least abnormally dry conditions by the summer's end with nearly half of the
287 region, especially the Great Plains, experiencing severe drought (Hoerling et al., 2013). This period
288 lacked the usual abundance of slow-soaking precipitation-bearing systems and evening
289 thunderstorms along the Great Plains, and as a result, surface moisture conditions greatly
290 deteriorated. GRACE data was used to identify this massive event (Humphrey et al., 2016). Most
291 importantly, GRACE TWS data helped identify the recovery time. In March 2013, heavy winter rains
292 broke a three-year pattern of meteorological drought in much of the southeastern United States,
293 while drought conditions still plagued the Great Plains and other parts of the United States. Chew
294 and Small (2014) found that standard drought indices misrepresent the recovery time from the
295 drought, putting it much earlier than the one obtained with the auxiliary information of GRACE
296 TWS. Accurate understanding of drought onset and recovery time is critical because drought
297 impacts grain and wheat prices (Boyer et al., 2013). A large disruption to production of these crops
298 can have a substantial impact on international grain markets. Also visible in **Figure 2** are the
299 droughts during the year 2007–2009 over east United States. Houborg et al. (2012) demonstrated
300 the capabilities of using GRACE data assimilation for characterizing the hydrological drought (more
301 discussion in Section 3.1.2). Further, the 2010–2013 drought in Texas is shown in **Figure 2** and was
302 described by Long et al. (2013).

303

304

305 *Africa*

306 **Figure 2** identifies the 2006–2007 dry conditions over an extended area around the Lake
307 Victoria (Swenson and Wahr 2009). The 2006–2008 Zambezi basin (Thomas et al. 2014) and Lake
308 Victoria droughts are captured as one large-scale and spatially contiguous event. Droughts in East
309 Africa are recurring phenomena with significant humanitarian impacts. GRACE total water storage
310 estimates reveal that water storage declined in much of East Africa by up to 60 mm/year (Swenson
311 and Wahr 2009) during the 2006-2007 drought. The complex and highly variant nature of many
312 hydrometeorological drivers such as ENSO, sea surface temperature (SST) and land–atmosphere
313 feedback adds to the daunting challenge of drought monitoring and forecasting in Africa. The 2010-
314 2011 drought of the Horn of Africa is not shown in **Figure 2** but it was identified using GRACE in
315 previous studies (e.g., Anderson et al., 2012) to characterize its temporal and spatial evolution.

316

317 *Eurasia*

318 Hydrological droughts are common in Europe, and several episodes of severe droughts,
319 including the 2003 drought (spreading across western and central Europe) and the 2007-2008
320 droughts (affecting southern and southwestern Europe) were detected by GRACE TWS (Li et al.,
321 2012). In particular, the 2003 event was associated with the 2003 European heat wave (Rebetez et
322 al., 2006). For most of Europe, TWS values were relatively high at the beginning of 2003 due to
323 heavy precipitation in summer and autumn of 2002, but they decreased very rapidly in the period
324 February–August, resulting in very dry conditions during the entire summer of 2003. The soil
325 drying in 2003 exceeded the long-term average by far (Herrera et al., 2010). Following the 2003
326 drought and heat wave, forest fires burned a large area of Siberia (Herrera et al., 2010). Drought
327 conditions can also be found in northern India for the period 2009–2010 (**Figure 2**). The year 2009
328 was the driest year of the decade for this region in terms of precipitation (Chen et al., 2014) and
329 resulted in higher groundwater abstraction rates (Rodell et al., 2009).

330 **Figure 2** identifies the 2004 drought in southeast China, around the Yangtze River basin.
331 The Yangtze River is experiencing an increasing trend in terms of the frequency of extreme events
332 (Dai et al., 2008), which often leads to severe reductions in crop outputs, along with other related
333 social and economic losses (Chao et al., 2016). Other severe drought events were identified in 2006
334 and 2011 (Sun et al., 2018). Previous works based on the analysis of GRACE data quantify a
335 terrestrial water storage deficit of -621; -617, -192 mm for the 2004, 2006, and 2011 droughts
336 respectively (Chao et al., 2016; Sun et al., 2018).

337 The Sumatra region exhibits a minimum in 2004 (**Figure 2**). However, this is an artifact
338 caused by the 2004 earthquake, with GRACE observing changes in the gravity field due to crustal
339 dilatation and vertical displacement of Earth's layered density structure (Han et al., 2006).

340

341 Australia

342 In Australia, multiyear droughts have been related to precipitation deficits (García-García et
343 al. 2011). Van Dijk et al. (2013) explain drivers of the drought and its impacts. These were analyzed
344 using climate, water, economic, and remote sensing data combined with biophysical modeling.
345 ENSO explained two third of the rainfall deficit, and a contribution of global climate change remains
346 plausible. The millennium drought (2001-2009) was the worst drought on record for southeast
347 Australia (Van Dijk et al., 2013). It has led to the almost complete drying of surface water resources,
348 which account for most of the water used for irrigation and domestic purposes. Using GRACE data,
349 Lebalnc et al. (2009) show the propagation of the water deficit through the hydrological cycle and
350 the rise of different types of drought.

351

352 3.1.2. The Potential for using GRACE in Monitoring and Predicting Droughts

353 Currently, standard drought quantitation methods and products including the U.S. Drought
354 Monitor (USDM) rely heavily on in situ observations of precipitation, streamflow, snowpack data,

355 and subjective human based judgments (Rodell, 2012). USDM drought maps are published on a
356 weekly basis by a team of authors and widely considered to be the premier US drought products
357 available for use by governments, farmers and other stakeholders, and the public, despite limited
358 groundwater and soil moisture data as direct inputs. Although meteorological drought is defined as
359 an extended period with deficient precipitation, hydrological and agricultural droughts are also
360 influenced by precursor conditions of groundwater and soil moisture. Surface moisture conditions
361 can fluctuate quickly with the weather, while the deeper components of TWS (e.g., groundwater)
362 are well suited to drought quantification, particularly hydrologic droughts, because they integrate
363 meteorological conditions over timescales of weeks to years (Rodell, 2012). Prior to USDM use of
364 GRACE data assimilation based drought indices (Houburg et al., 2012), drought products did not
365 incorporate systematic observations of soil moisture, groundwater, or total TWS. Groundwater
366 storage and shallow and deep soil moisture are still major gaps in current drought monitoring
367 capabilities and monitoring of droughts has suffered from lack of reliable information on the water
368 stored below the uppermost soil layer. Remote sensing-based drought indices have opened a new
369 path forward in drought monitoring and detection (Niemeyer, 2008), allowing accurate spatial
370 information to be obtained with global or regional coverage with high reliability and a high
371 repetition rate (Sun et al., 2018). In particular, since GRACE measures the water storage changes in
372 the entire profile, it provides valuable information on drought conditions beyond what can be seen
373 at the surface (Li et al., 2012). Further, given that GRACE offers information on the total water
374 storage deficit it can be used to estimate the amount of water (precipitation) needed to recover
375 from drought events (Thomas et al., 2014; Aghakouchak et al., 2014).

376

377 3.2 Floods

378 Flood events are projected to become more frequent as global warming amplifies the
379 atmosphere's water holding capacity, increasing the occurrence of extreme precipitation events

380 (Slater and Villarini 2016; Groisman, 2012; Wang et al., 2017). Many countries have developed
381 flood alert systems (Molodtsova et al., 2016), such as the European Flood Alert System (Bartholmes
382 et al., 2009) and the US National Weather Service Automated Flood Warning System (Scawthorn,
383 1999). While most of these warning systems rely on a dense network of gauging stations, a
384 significant portion of the economic losses caused by floods occur in developing countries where
385 ground flood monitoring and management programs are still inefficient (Molodtsova et al., 2016).
386 To augment ground-based observations, flood monitoring has increasingly relied on products
387 based on space-borne sensor observations (i.e., remote sensing). Among the remote sensing
388 products that have been used for flood monitoring, data from the GRACE mission are unique
389 because the total amount of terrestrial water can be directly measured (Molodtsova et al., 2016).
390 The terrestrial water storage signal relates to the ability of the land surface to absorb and process
391 water and accounts for the water in plants, groundwater, soil moisture and snow (Reager and
392 Famiglietti 2009). Over the course of a year, a region can transition between its minimum and
393 maximum TWS due to the annual cycle of precipitation. When the region is near the maximum, it
394 can store and process only a finite amount of water before the saturated ground will force
395 additional precipitation to runoff (Reager and Famiglietti 2009). Generally, the land surface
396 modulates the connection between precipitation and runoff generation through two basic
397 mechanisms: infiltration limitation and saturation excess. During floods, one of these two
398 mechanisms is typically identified as a driver based on the pre-flood conditions and the nature of
399 the precipitation event (Reager et al., 2015). That is, the pre-rainfall event wetness of a watershed
400 can determine its response to rainfall (Sayama et al., 2011; Kirchner 2009; Brutsaert 2008), leading
401 to variability in flood generation (Li et al., 2002). Salter and Villarini (2016) show that flood
402 patterns are dependent on the overall wetness and potential water storage, with fundamental
403 implications for water resources management, agriculture, insurance, navigation, ecology, and
404 populations living in flood-affected areas.

405

406 3.2.1. Flood Potential from GRACE

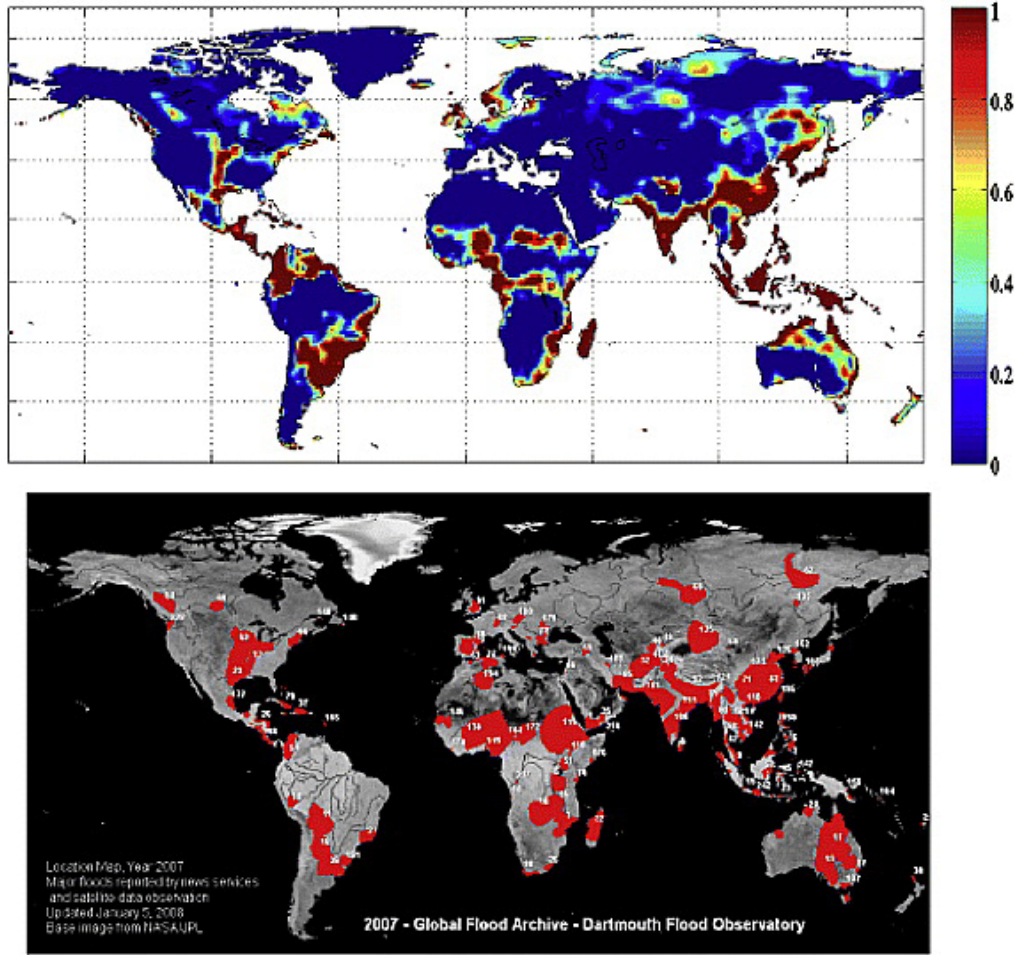
407 Reager and Famiglietti (2009) introduced the concept of “flood potential” to highlight the
408 information relevant for regional flooding contained in the GRACE extreme (wet) TWS values. TWS
409 that is near its maximum can be a harbinger of future flood events at several months lead-time
410 (Reager and Famiglietti 2009). The concept of flood potential has been used in several studies
411 (Section 3.2.2) to analyze flood risk in different watersheds around the world.

412 Reager and Famiglietti (2009) assume that the regional storage capacity can be
413 approximated by the historic record maximum in the GRACE TWS storage anomaly time series to
414 give a quantitative estimate (in cm) of the saturation point of the regional land surface. In a
415 nutshell, GRACE time series can be used to calculate an effective maximum storage capacity in each
416 region. Reager and Famiglietti (2009) isolate, temporally and spatially, those months in which a
417 high percentage of the storage capacity is achieved and high precipitation continues. Finally, they
418 normalized this new dataset to remove regional heterogeneity and create a global flood potential
419 index. The resulting flood potential amount is the quantity of incoming water that exceeds the
420 storage capacity for the current month based on the regionally observed storage anomaly maxima.
421 Similar to a traditional ‘bucket model’, when this quantity exceeds zero, flooding is likely to occur.

422 **Figure 3a** shows a global map of the flood index for the year 2007 as derived by Reager and
423 Famiglietti (2009). This is compared to the Dartmouth Flood Observatory map of reported floods
424 (**Figure 3b**). The Dartmouth Flood Observatory catalogues historic floods based on satellite
425 observations, weather service and news reports (<https://www.dartmouth.edu/~floods/>). The red
426 areas in **Figure 3b** indicate observed floods during 2007. While the GRACE derived flood index
427 (**Figure 3a**) misses some flooded regions in Africa and Asia, it is generally successful at predicting
428 large-scale flood-affected areas. The index captures the general patterns of flooding on most
429 continents, and captures some rather high spatial resolution structure, including events on the

430 southernmost tip of Africa and the unique 'T' shape of Mississippi river flooding (Reager and
431 Famiglietti, 2009). Further, Reager et al. (2014) demonstrate the ability of the flood potential
432 concept to derive longer lead times (as much as 5–11 months in advance) in flood warnings at a
433 regional scale (e.g. for the Missouri 2011, the Columbia River 2011 and Indus River 2010 flood
434 events).

435 However, several limitations still exist for using satellite gravimetry in an operational flood
436 prediction mode (Reager et al., 2015). The prevailing limitations are: (1) coarse spatial resolution
437 (~150,000 km², Rowlands et al., 2005; Swenson et al., 2006); (2) the aggregated observation of
438 multiple water storage components (i.e., snow, soil moisture, and groundwater) as a single
439 integrated value for each grid cell; and (3) latency in data product processing and release (2–4
440 months lag for GRACE and at least ten days for GRACE-FO). These obstacles make many
441 applications difficult, as water resource management tends to occur at small watershed scales and
442 on daily to weekly timescales. For this reason, similarly to the drought monitoring work by
443 Houburg et al. (2012), data assimilation can be used as a tool to partially overcome these
444 limitations. In their work, Reager et al. (2015) assimilate GRACE data within the catchment land
445 surface model and evaluate the assimilation scheme performance under flood conditions. The
446 assimilation results made the model wetter in the months preceding flood, thus increasing the
447 model capability to predict floods.



448

449 **Figure 3. A comparison of the (top) 2007 flood index maxima and (bottom) 2007 Dartmouth Flood**
 450 **Observatory reported floods. (source Reager and Famiglietti 2009)**
 451

452

453 3.2.2. Historical Flood Events Characterized by GRACE

454 The investigation of GRACE data to characterize flooding events has not been exploited as
 455 much as the characterization of drought events. This section lists historical flooding events that
 456 have been investigated with the use of GRACE data.

457 dutt Vishwakarma et al. (2013) discussed two major flooding events in India, one being the
 458 2005 monsoon flooding in Mumbai and nearby states and other being the flood experienced by
 459 Bihar in 2008. GRACE detected these two flooding events at large spatial scale. Long et al. (2014)
 460 used the flood potential index derived by Reager and Famiglietti (2009) to characterize the 2008

461 severe flood in southwest China. Chinnasamy (2017) develop a regression model between GRACE
462 data and observed discharge flow. Their model was tested to predict the 2008 Koshi floods, India.
463 Their results indicate that the saturation of water storage units in the basin play a vital role in the
464 prediction of peak floods and their lead times. Chen et al. (2010) used GRACE to identify the
465 Amazon River 2009 flood event, which caused many casualties, and its connection to ENSO. Sun et
466 al. (2017) use GRACE data to evaluate the flood potential index (Reager and Famiglietti 2009) in the
467 Yangtze River Basin of China. Zhou et al., (2017) also investigated the potentials for using GRACE
468 data for identifying and predicting floods in the Yangtze River Basin. In particular, the 2010 flood
469 was identified as the most serious disaster during the study period, with discharge and
470 precipitation values 37.95% and 19.44% higher, respectively, than multi-year average values for
471 the same period. Zhou et al. (2017) highlight that while the GRACE derived flood potential index can
472 identify extremes for large floods, it is currently not suitable for smaller and/or short-term flood
473 events (Sun et al., 2017). Tangdamrongsub et al. (2016) used GRACE data to quantify flooding of the
474 Tonlé ap basin, Cambodia between 2002 and 2014. For this region, the 2011 and 2013 flood events
475 were clearly identified by GRACE. The basin-averaged TWS values for these two events were 42 cm
476 (40% higher than the long-term mean peak value) and 36 cm (34% higher) equivalent water
477 height, respectively. In May and June of 2011, a large flood crest moved down the Mississippi from a
478 combination of snowmelt and heavy spring rains in the Missouri river basin. Flows in the Missouri
479 were characterized as a 500-year event. Red River Landing, near the mouth of the Mississippi, went
480 above flood stage on 19 March and did not fall below flood stage until 25 June. Reager et al. (2014)
481 and Wang et al. (2014) investigate this flood event using GRACE data and they indicate that analysis
482 of TWS observations has the potential for providing spatially distributed warning information.
483 Similar conclusions were derived for the Columbia River flood event in May-June 2011, and the
484 Indus River flood in 2010.

485 **4. Conclusions**

486
487 Extremes in water storage are often manifested as drought and flooding events, driven by
488 the surplus or deficit of water stored in a river basin or an aquifer. These events are projected to
489 become more frequent as a result of global warming (Pachauri et al., 2014). The existing in situ
490 observing networks are not sufficient to detect and monitor these extremes in the total amount of
491 water stored in a region. GRACE observations have helped to fill this information gap because it has
492 provided an unprecedented, holistic view of terrestrial water storage variations. GRACE Follow On,
493 launched in May 2018, will extend that important data record.

494 GRACE contributed to regional drought characterization by measuring water storage
495 deficits drought-stricken areas. It also provided information useful for predicting regional flood
496 potential. The concepts of flood potential and water storage deficit have been used in several
497 studies to characterize the extremes observed by GRACE. This book chapter reviewed many of the
498 most significant studies.

499 Limitations still exist for using GRACE and GRACE Follow On data in an operational drought
500 or flood prediction mode. The major limitations are related to the relatively coarse spatial and
501 temporal resolutions of the GRACE observations and the fact that TWS is an aggregated observation
502 of multiple water storage components (i.e., snow, soil moisture, and groundwater). Latency in the
503 delivery of GRACE data is also a serious issue, but that is expected to be mitigated by the availability
504 of low latency data products derived from GRACE Follow On (e.g., Sakumura et al., 2016). These
505 limitations can be addressed through the combined use of observed TWS and models, i.e., via data
506 assimilation (e.g., Zaitchik et al., 2008; Giroto et al., 2016).

507
508

509 **References**

- 510 Abelen, S., Seitz, F., Abarca-del-Rio, R., & Güntner, A. (2015). Droughts and floods in the La Plata
511 basin in soil moisture data and GRACE. *Remote Sensing*, 7(6), 7324-7349.
512
- 513 AghaKouchak, A., Cheng, L., Mazdidasni, O., & Farahmand, A. (2014). Global warming and changes in
514 risk of concurrent climate extremes: Insights from the 2014 California drought. *Geophysical
515 Research Letters*, 41(24), 8847-8852.
516
- 517 Anderson, R. G., Lo, M. H., & Famiglietti, J. S. (2012). Assessing surface water consumption using
518 remotely-sensed groundwater, evapotranspiration, and precipitation. *Geophysical Research
519 Letters*, 39(16).
520
- 521 Bartholmes, J. C., Thielen, J., Ramos, M. H., & Gentilini, S. (2009). The european flood alert system
522 EFAS-Part 2: Statistical skill assessment of probabilistic and deterministic operational
523 forecasts. *Hydrology and Earth System Sciences*, 13(2), 141-153.
524
- 525 Boyer, J. S., Byrne, P., Cassman, K. G., Cooper, M., Delmer, D., Greene, T., ... & Lafitte, R. (2013). The US
526 drought of 2012 in perspective: A call to action. *Global Food Security*, 2(3), 139-143.
527
- 528 Brutsaert, W. Long-term groundwater storage trends estimated from streamflow records: Climatic
529 perspective. *Wat. Resour. Res.* 44, W02409 (2008).
530
- 531 Cao, Y., Nan, Z., & Cheng, G. (2015). GRACE gravity satellite observations of terrestrial water storage
532 changes for drought characterization in the arid land of northwestern China. *Remote
533 Sensing*, 7(1), 1021-1047.
534
- 535 Chao, N., Wang, Z., Jiang, W., & Chao, D. (2016). A quantitative approach for hydrological drought
536 characterization in southwestern China using. *Hydrogeology Journal*, 24(4), 893-903.
537
- 538 Chen, J. L., Wilson, C. R., Tapley, B. D., Longuevergne, L., Yang, Z. L., & Scanlon, B. R. (2010). Recent La
539 Plata basin drought conditions observed by satellite gravimetry. *Journal of Geophysical
540 Research: Atmospheres*, 115(D22).
541
- 542 Chen, J., Famiglietti, J. S., Scanlon, B. R., & Rodell, M. (2016). Groundwater storage changes: present
543 status from GRACE observations. *Surveys in Geophysics*, 37(2), 397-417.
544
- 545 Chew, C. C., & Small, E. E. (2014). Terrestrial water storage response to the 2012 drought estimated
546 from GPS vertical position anomalies. *Geophysical Research Letters*, 41(17), 6145-6151.
547
- 548 Chinnasamy, P. (2017), Inference of basin flood potential using nonlinear hysteresis effect of basin
549 water storage: case study of the Koshi basin, *Hydrology Research*, 48(6), 1554-
550 1565. <https://dx.doi.org/10.2166/nh.2016.268>.
551
- 552 Crow, W. T., Bindlish, R., & Jackson, T. J. (2005). The added value of spaceborne passive microwave
553 soil moisture retrievals for forecasting rainfall-runoff partitioning. *Geophysical Research
554 Letters*, 32(18).
555

556 Dai, Z., Du, J., Li, J., Li, W., & Chen, J. (2008). Runoff characteristics of the Changjiang River during
557 2006: effect of extreme drought and the impounding of the Three Gorges Dam. *Geophysical*
558 *Research Letters*, 35(7).
559

560 Davidson, E. A., de Araújo, A. C., Artaxo, P., Balch, J. K., Brown, I. F., Bustamante, M. M., ... & Munger, J.
561 W. (2012). The Amazon basin in transition. *Nature*, 481(7381), 321.
562

563 Diffenbaugh, N.S.; Scherer, M. Observational and model evidence of global emergence of permanent,
564 unprecedented heat in the 20th and 21st centuries. *Clim. Chang.* 2011, 107, 615–624. [CrossRef]
565 [PubMed]
566

567 D’Odorico, P.; Laio, F.; Ridolfi, L. Does globalization of water reduce societal resilience to drought?
568 *Geophys. Res. Lett.* 2010, 37. [CrossRef]
569

570 dutt Vishwakarma, B., Jain, K., Sneeuw, N., & Devaraju, B. (2013). Mumbai 2005, Bihar 2008 flood
571 reflected in mass changes seen by GRACE satellites. *Journal of the Indian Society of Remote*
572 *Sensing*, 41(3), 687-695.
573

574 Entekhabi, D., I. Rodriguez-Iturbe, and F. Castelli (1996), Mutual interaction of soil moisture state
575 and atmospheric process, *J. Hydrol.*, 184, 3–17.
576

577 Famiglietti, J. S. (2004). Remote sensing of terrestrial water storage, soil moisture and surface
578 waters. *The state of the planet: frontiers and challenges in geophysics*, 197-207.
579

580 Famiglietti, J. S., Lo, M., Ho, S. L., Bethune, J., Anderson, K. J., Syed, T. H., ... & Rodell, M. (2011).
581 Satellites measure recent rates of groundwater depletion in California's Central
582 Valley. *Geophysical Research Letters*, 38(3).
583

584 Famiglietti, J. S. (2014). The global groundwater crisis. *Nature Climate Change*, 4(11), 945.
585

586 Faunt, C. C., Hanson, R. T., & Belitz, K. (2009). Chapter A. Introduction, Overview of Hydrogeology,
587 and Textural Model of California's Central Valley. *US Geological Survey professional paper*,
588 (1766).
589

590 Frappart, F., Papa, F., da Silva, J. S., Ramillien, G., Prigent, C., Seyler, F., & Calmant, S. (2012). Surface
591 freshwater storage and dynamics in the Amazon basin during the 2005 exceptional
592 drought. *Environmental Research Letters*, 7(4), 044010.
593

594 Galloway, D., & Riley, F. S. (1999). San Joaquin Valley, California. *Land subsidence in the United*
595 *States: US Geological Survey Circular*, 1182, 23-34.
596

597 García-García, D., Ummenhofer, C. C., & Zlotnicki, V. (2011). Australian water mass variations from
598 GRACE data linked to Indo-Pacific climate variability. *Remote Sensing of Environment*, 115(9),
599 2175-2183.
600

601 García-Herrera, R., Díaz, J., Trigo, R. M., Luterbacher, J., & Fischer, E. M. (2010). A review of the
602 European summer heat wave of 2003. *Critical Reviews in Environmental Science and*
603 *Technology*, 40(4), 267-306.
604

605 Getirana, A. (2016). Extreme water deficit in Brazil detected from space. *Journal of*
606 *Hydrometeorology*, 17(2), 591-599.
607
608 Getirana, A., Kumar, S., Giroto, M., & Rodell, M. (2017). Rivers and floodplains as key components of
609 global terrestrial water storage variability. *Geophysical Research Letters*, 44(20).
610
611 Giroto, M., Margulis, S. A., & Durand, M. (2014). Probabilistic SWE reanalysis as a generalization of
612 deterministic SWE reconstruction techniques. *Hydrological processes*, 28(12), 3875-3895.
613
614 Giroto, M., De Lannoy, G. J., Reichle, R. H., & Rodell, M. (2016). Assimilation of gridded terrestrial
615 water storage observations from GRACE into a land surface model. *Water Resources Research*,
616 52(5), 4164-4183.
617
618 Giroto, M., De Lannoy, G. J., Reichle, R. H., Rodell, M., Draper, C., Bhanja, S. N., & Mukherjee, A.
619 (2017). Benefits and pitfalls of GRACE data assimilation: A case study of terrestrial water
620 storage depletion in India. *Geophysical research letters*, 44(9), 4107-4115.
621
622 Gleeson, T., Wada, Y., Bierkens, M. F., & van Beek, L. P. (2012). Water balance of global aquifers
623 revealed by groundwater footprint. *Nature*, 488(7410), 197.
624
625 Groisman, P. Y., Knight, R. W., & Karl, T. R. (2012). Changes in intense precipitation over the central
626 United States. *Journal of Hydrometeorology*, 13(1), 47-66.
627
628 Hall, D. K., Chang, A. T., & Siddalingaiah, H. (1988). Reflectances of glaciers as calculated using
629 Landsat-5 Thematic Mapper data. *Remote Sensing of Environment*, 25(3), 311-321.
630
631 Han, S. C., Shum, C. K., Bevis, M., Ji, C. & Kuo, C. Y. Crustal dilatation observed by GRACE after the 2004
632 Sumatra-Andaman earthquake. *Science* 313, 658–662, doi: 10.1126/science.1128661 (2006)
633
634 Hoerling, M., Eischeid, J., Kumar, A., Leung, R., Mariotti, A., Mo, K., ... & Seager, R. (2014). Causes and
635 predictability of the 2012 Great Plains drought. *Bulletin of the American Meteorological*
636 *Society*, 95(2), 269-282.
637
638 Houborg, R., Rodell, M., Li, B., Reichle, R., & Zaitchik, B. F. (2012). Drought indicators based on
639 model-assimilated Gravity Recovery and Climate Experiment (GRACE) terrestrial water storage
640 observations. *Water Resources Research*, 48(7).
641
642 Humphrey, V., Gudmundsson, L., & Seneviratne, S. I. (2016). Assessing global water storage
643 variability from GRACE: Trends, seasonal cycle, subseasonal anomalies and extremes. *Surveys in*
644 *geophysics*, 37(2), 357-395.
645
646 Kirchner, J. W. Catchments as simple dynamical systems: Catchment characterization, rainfall-
647 runoff modeling, and doing hydrology backwards. *Wat. Resour. Res.* 45, W02429 (2009).
648
649 Kusche, J., Eicker, A., Forootan, E., Springer, A., & Longuevergne, L. (2016). Mapping probabilities of
650 extreme continental water storage changes from space gravimetry. *Geophysical Research*
651 *Letters*, 43(15), 8026-8034.
652

653 Leblanc, M. J., Tregoning, P., Ramillien, G., Tweed, S. O., & Fakes, A. (2009). Basin-scale, integrated
654 observations of the early 21st century multiyear drought in southeast Australia. *Water*
655 *resources research*, 45(4).
656

657 Li, B., Rodell, M., Zaitchik, B. F., Reichle, R. H., Koster, R. D., & van Dam, T. M. (2012). Assimilation of
658 GRACE terrestrial water storage into a land surface model: Evaluation and potential value for
659 drought monitoring in western and central Europe. *Journal of Hydrology*, 446, 103-115.
660

661 Li, B., M. Rodell, and J.S. Famiglietti (2015), Groundwater variability across temporal and spatial
662 scales in the central and northeastern U.S., *J. Hydrology*, 525, 769-780,
663 doi:10.1016/j.jhydrol.2015.04.033,.
664

665 Li, L. & Simonovic, S. P. (2002). System dynamics model for predicting floods from snowmelt in
666 North American prairie watersheds. *Hydrol. Process.* 16, 2645–2666.
667

668 Long, D., Shen, Y., Sun, A., Hong, Y., Longuevergne, L., Yang, Y., ... & Chen, L. (2014). Drought and
669 flood monitoring for a large karst plateau in Southwest China using extended GRACE
670 data. *Remote Sensing of Environment*, 155, 145-160.
671

672 Luthcke, S.B., T.J. Sabaka, B.D. Loomis, et al. (2013), Antarctica, Greenland and Gulf of Alaska land
673 ice evolution from an iterated GRACE global mascon solution, *J. Glac.*; 59(216), 613-
674 631, doi:10.3189/2013Jog12J147
675

676 Margulis, S. A., Cortés, G., Giroto, M., Huning, L. S., Li, D., & Durand, M. (2016). Characterizing the
677 extreme 2015 snowpack deficit in the Sierra Nevada (USA) and the implications for drought
678 recovery. *Geophysical Research Letters*, 43(12), 6341-6349.
679

680 Milly, P. C. D., and K. A. Dunne, (1994) Sensitivity of the global water cycle to the water-holding
681 capacity of the land, *J. Clim.*, 7, 506–526.
682

683 Molodtsova, T., Molodtsov, S., Kirilenko, A., Zhang, X., & VanLooy, J. (2016). Evaluating flood
684 potential with GRACE in the United States. *Natural Hazards and Earth System Sciences*, 16(4),
685 1011-1018
686

687 Niemeyer, S. (2008). New drought indices. *Options Méditerranéennes. Série A: Séminaires*
688 *Méditerranéens*, 80, 267-274.
689

690 Pachauri, R. K., Allen, M. R., Barros, V. R., Broome, J., Cramer, W., Christ, R., ... & Dubash, N. K.
691 (2014). *Climate change 2014: synthesis report. Contribution of Working Groups I, II and III to the*
692 *fifth assessment report of the Intergovernmental Panel on Climate Change* (p. 151). IPCC.
693

694 Reager, J. T., & Famiglietti, J. S. (2009). Global terrestrial water storage capacity and flood potential
695 using GRACE. *Geophysical Research Letters*, 36(23).
696

697 Reager, J. T., Thomas, B. F., & Famiglietti, J. S. (2014). River basin flood potential inferred using
698 GRACE gravity observations at several months lead time. *Nature Geoscience*, 7(8), 588.
699

700 Reager, J. T., Thomas, A. C., Sproles, E. A., Rodell, M., Beaudoin, H. K., Li, B., & Famiglietti, J. S.
701 (2015). Assimilation of GRACE terrestrial water storage observations into a land surface model
702 for the assessment of regional flood potential. *Remote Sensing*, 7(11), 14663-14679.

703
704 Rebetetz, M., Mayer, H., Dupont, O., Schindler, D., Gartner, K., Kropp, J. P., & Menzel, A. (2006). Heat
705 and drought 2003 in Europe: a climate synthesis. *Annals of Forest Science*, 63(6), 569-577.
706
707 Richey, A.S., B.F. Thomas, M.-H. Lo, S. Swenson, M. Rodell, and J.S. Famiglietti, (2015). Uncertainty in
708 global groundwater storage estimates in a total groundwater stress framework, *Wat. Resour.*
709 *Res.*, 51, 5198–5216, doi:10.1002/2015WR017351.
710
711 Rippey, B. R. (2015). The US drought of 2012. *Weather and Climate Extremes*, 10, 57-64.
712
713 Rodell, M., & Famiglietti, J. S. (1999). Detectability of variations in continental water storage from
714 satellite observations of the time dependent gravity field. *Water Resources Research*, 35(9),
715 2705-2723.
716
717 Rodell, M., & Famiglietti, J. S. (2001). An analysis of terrestrial water storage variations in Illinois
718 with implications for the Gravity Recovery and Climate Experiment (GRACE). *Water Resources*
719 *Research*, 37(5), 1327-1339.
720
721 Rodell, M., Chao, B. F., Au, A. Y., Kimball, J. S., & McDonald, K. C. (2005). Global biomass variation and
722 its geodynamic effects: 1982–98. *Earth Interactions*, 9(2), 1-19.
723
724 Rodell, M., Velicogna, I., & Famiglietti, J. S. (2009). Satellite-based estimates of groundwater
725 depletion in India. *Nature*, 460(7258), 999.
726
727 Rodell, M. (2012). 11 Satellite Gravimetry Applied to Drought Monitoring. *Remote Sensing of*
728 *Drought: Innovative Monitoring Approaches*, 261.
729
730 Rowlands, D. D., Luthcke, S. B., Klosko, S. M., Lemoine, F. G., Chinn, D. S., McCarthy, J. J., ... &
731 Anderson, O. B. (2005). Resolving mass flux at high spatial and temporal resolution using
732 GRACE intersatellite measurements. *Geophysical Research Letters*, 32(4).
733
734 Sakumura, C., Bettadpur, S., Save, H., & McCullough, C. (2016). High-frequency terrestrial water
735 storage signal capture via a regularized sliding window mascon product from GRACE. *Journal of*
736 *Geophysical Research: Solid Earth*, 121(5), 4014-4030.
737
738 Sayama, T., McDonnell, J. J., Dhakal, A. & Sullivan, K. How much water can a watershed store? *Hydrol.*
739 *Process.* 25, 3899–3908 (2011).
740
741 Save, H., S. Bettadpur, and B. D. Tapley (2012), Reducing errors in the GRACE gravity solutions
742 using regularization, *J. Geod.*, doi:10.1007/s00190-012-0548-5
743
744 Scanlon, B. R., Longuevergne, L., & Long, D. (2012a). Ground referencing GRACE satellite estimates
745 of groundwater storage changes in the California Central Valley, USA. *Water Resources*
746 *Research*, 48(4).
747
748 Scanlon, B. R., Faunt, C. C., Longuevergne, L., Reedy, R. C., Alley, W. M., McGuire, V. L., & McMahon, P.
749 B. (2012b). Groundwater depletion and sustainability of irrigation in the US High Plains and
750 Central Valley. *Proceedings of the national academy of sciences*, 109(24), 9320-9325.
751

752 Scawthorn, C. (1999). Modeling flood events in the US. *Proceedings of the EuroConference on Global*
753 *Change and Catastrophe Risk Management, International Institute for Advanced Systems Analysis,*
754 *Laxenburg, Austria.*
755

756 Schmutge, T. J., Kustas, W. P., Ritchie, J. C., Jackson, T. J., & Rango, A. (2002). Remote sensing in
757 hydrology. *Advances in water resources, 25*(8-12), 1367-1385.
758

759 Seneviratne, S. (2003). *Terrestrial water storage: a critical variable for mid-latitude climate and*
760 *climate change* (Doctoral dissertation, ETH Zurich).
761

762 Seneviratne, S.I., Corti, T., Davin, E.L., Hirschi, M., Jaeger, E.B., Lehner, I., Orlowsky, B. and Teuling,
763 A.J., (2010). Investigating soil moisture–climate interactions in a changing climate: A review.
764 *Earth-Science Reviews, 99*(3-4), pp.125-161.
765

766 Slater, L. J., & Villarini, G. (2016). Recent trends in US flood risk. *Geophysical Research*
767 *Letters, 43*(24).
768

769 Sordo-Ward, A., Bejarano, M. D., Iglesias, A., Asenjo, V., & Garrote, L. (2017). Analysis of Current and
770 Future SPEI Droughts in the La Plata Basin Based on Results from the Regional Eta Climate
771 Model. *Water, 9*(11), 857.
772

773 Sun, A. Y., Scanlon, B. R., AghaKouchak, A., & Zhang, Z. (2017). Using GRACE Satellite Gravimetry for
774 Assessing Large-Scale Hydrologic Extremes. *Remote Sensing, 9*(12), 1287.
775

776 Sun, Z., X. Zhu, Y. Pan, and J. Zhang (2017), Assessing terrestrial water storage and flood potential
777 using GRACE data in the Yangtze River Basin, China, *Remote Sensing,*
778 *9*(10). <https://dx.doi.org/10.3390/rs9101011>.
779

780 Sun Z., Zhu X., Pan Y, Zhang J., Liu X. Drought evaluation using the GRACE terrestrial water storage
781 deficit over the Yangtze River Basin, China. *Science of The Total Environment, 2018.*
782 <https://doi.org/10.1016/j.scitotenv.2018.03.292>
783

784 Svoboda, M., LeComte, D., Hayes, M., Heim, R., Gleason, K., Angel, J., ... & Miskus, D. (2002). The
785 drought monitor. *Bulletin of the American Meteorological Society, 83*(8), 1181-1190.
786

787 Swenson, S., & Wahr, J. (2006). Post-processing removal of correlated errors in GRACE
788 data. *Geophysical Research Letters, 33*(8).
789

790 Syed, T. H., Famiglietti, J. S., Rodell, M., Chen, J., & Wilson, C. R. (2008). Analysis of terrestrial water
791 storage changes from GRACE and GLDAS. *Water Resources Research, 44*(2).
792

793 Tangdamrongsub, N., Ditmar, P. G., Steele-Dunne, S. C., Gunter, B. C., & Sutanudjaja, E. H. (2016).
794 Assessing total water storage and identifying flood events over Tonlé Sap basin in Cambodia
795 using GRACE and MODIS satellite observations combined with hydrological models. *Remote*
796 *Sensing of Environment, 181,* 162-173.
797

798 Tapley, B. D., Bettadpur, S., Ries, J. C., Thompson, P. F., & Watkins, M. M. (2004). GRACE
799 measurements of mass variability in the Earth system. *Science, 305*(5683), 503-505.
800

801 Thomas, A. C., Reager, J. T., Famiglietti, J. S., & Rodell, M. (2014). A GRACE-based water storage
802 deficit approach for hydrological drought characterization. *Geophysical Research Letters*, 41(5),
803 1537-1545.
804

805 Dijk, A. I., Beck, H. E., Crosbie, R. S., Jeu, R. A., Liu, Y. Y., Podger, G. M., ... & Viney, N. R. (2013). The
806 Millennium Drought in southeast Australia (2001–2009): Natural and human causes and
807 implications for water resources, ecosystems, economy, and society. *Water Resources*
808 *Research*, 49(2), 1040-1057.
809

810 Wada, Y., van Beek, L. P., van Kempen, C. M., Reckman, J. W., Vasak, S., & Bierkens, M. F. (2010).
811 Global depletion of groundwater resources. *Geophysical research letters*, 37(20).
812

813 Wang, G., Wang, D., Trenberth, K. E., Erfanian, A., Yu, M., Bosilovich, M. G., & Parr, D. T. (2017). The
814 peak structure and future changes of the relationships between extreme precipitation and
815 temperature. *Nature Climate Change*, 7(4), 268.
816

817 Wang, S. Y., Hakala, K., Gillies, R. R., & Capehart, W. J. (2014). The Pacific quasi-decadal oscillation
818 (QDO): An important precursor toward anticipating major flood events in the Missouri River
819 Basin?. *Geophysical Research Letters*, 41(3), 991-997.
820

821 Wang, S., & Russell, H. A. (2016). Forecasting snowmelt-induced flooding using GRACE satellite
822 data: A case study for the Red River watershed. *Canadian Journal of Remote Sensing*, 42(3), 203-
823 213.
824

825 Wang, S., Zhou, F., & Russell, H. A. (2017). Estimating snow mass and peak river flows for the
826 mackenzie river basin using grace satellite observations. *Remote Sensing*, 9(3), 256.
827

828 Watkins, M. M., Wiese, D. N., Yuan, D. N., Boening, C., & Landerer, F. W. (2015). Improved methods
829 for observing Earth's time variable mass distribution with GRACE using spherical cap
830 mascons. *Journal of Geophysical Research: Solid Earth*, 120(4), 2648-2671.
831

832 Wahr, J., Molenaar, M., & Bryan, F. (1998). Time variability of the Earth's gravity field: Hydrological
833 and oceanic effects and their possible detection using GRACE. *Journal of Geophysical Research:*
834 *Solid Earth*, 103(B12), 30205-30229.
835

836 Wahr, J., Swenson, S., & Velicogna, I. (2006). Accuracy of GRACE mass estimates. *Geophysical*
837 *Research Letters*, 33(6).
838

839 Yi, H., & Wen, L. (2016). Satellite gravity measurement monitoring terrestrial water storage change
840 and drought in the continental United States. *Scientific reports*, 6, 19909.
841

842 Yirdaw, S. Z., Snelgrove, K. R., & Agboma, C. O. (2008). GRACE satellite observations of terrestrial
843 moisture changes for drought characterization in the Canadian Prairie. *Journal of*
844 *Hydrology*, 356(1-2), 84-92.
845

846 Zehe, E., Becker, R., Bárdossy, A., & Plate, E. (2005). Uncertainty of simulated catchment runoff
847 response in the presence of threshold processes: Role of initial soil moisture and precipitation.
848 *Journal of hydrology*, 315(1-4), 183-202.
849

850 Zhao, M., Velicogna, I., & Kimball, J. S. (2017). Satellite observations of regional drought severity in
851 the continental United States using GRACE-based terrestrial water storage changes. *Journal of*
852 *Climate*, 30(16), 6297-6308.

853
854 Zhou, H., Z. Luo, N. Tangdamrongsub, L. Wang, L. He, C. Xu, and Q. Li (2017), Characterizing drought
855 and flood events over the Yangtze River Basin using the HUST-Grace2016 solution and ancillary
856 data, *Remote Sensing*, 9(11). <https://dx.doi.org/10.3390/rs9111100>.

857